Southern Ocean bioproductivity during the last glacial cycle – new detection method and decadal-scale insight from the Scotia Sea

D. SPRENK[1]*, M. E. WEBER[1], G. KUHN[2], P. ROSÉN[3], M. FRANK[4], M. MOLINA-KESCHER[4], V. LIEBETRAU[4] & H.-G. RÖHLING[5]

[1]*Institute of Geology and Mineralogy, University of Cologne, Zuelpicher Str. 49a, D-50674 Cologne, Germany*

[2]*Alfred-Wegener-Institut Helmholtz-Zentrum für Polar und Meeresforschung, Am Alten Hafen 26, D-27568 Bremerhaven, Germany*

[3]*Climate Impacts Research Centre (CIRC), Umeå University, SE-981 07 Abisko, Sweden*

[4]*GEOMAR Helmholtz Centre for Ocean Research Kiel, Wischhofstr. 1-3, D-24148 Kiel, Germany*

[5]*LBEG Landesamt für Bergbau, Energie und Geologie, Stilleweg 2, D-30655 Hannover, Germany*

**Corresponding author (e-mail: dsprenk@uni-koeln.de)*

Abstract: We present biogenic opal flux records from two deep-sea sites in the Scotia Sea (MD07-3133 and MD07-3134) at decadal-scale resolution, covering the last glacial cycle. In addition to conventional and time-consuming biogenic opal measuring methods, we introduce new biogenic opal estimation methods derived from sediment colour b^*, wet bulk density, Si/Ti-count ratio and Fourier transform infrared spectroscopy (FTIRS). All methods capture the biogenic opal amplitude; however, FTIRS – a novel method for marine sediment – yields the most reliable results. ^{230}Th normalization data show strong differences in sediment focusing with intensified sediment focusing during glacial times. At MD07-3134 ^{230}Th normalized biogenic opal fluxes vary between 0.2 and 2.5 g cm^{-2} kyr^{-1}. Our biogenic opal flux records indicate bioproductivity changes in the Southern Ocean, strongly influenced by sea ice distribution and also summer sea surface temperature changes. South of the Antarctic Polar Front, lowest bioproductivity occurred during the Last Glacial Maximum when upwelling of mid-depth water was reduced and sea ice cover intensified. Around 17 ka, bioproductivity increased abruptly, corresponding to rising atmospheric CO_2 and decreasing seasonal sea ice coverage.

The Southern Ocean plays an important role in transferring carbon dioxide (CO_2) via wind-induced upwelling from the deep sea to the atmosphere (Toggweiler *et al.* 2006; Anderson *et al.* 2009) and is therefore one of the key regions from which to study climate change. Bioproductivity in the Southern Ocean is mainly controlled by the rate of upwelling of cold nutrient- and silica-rich water masses, the extent of sea ice coverage, and the availability of light and micronutrients (Dezileau *et al.* 2003; de Baar *et al.* 2005; Stenni *et al.* 2010). Thus, bioproductivity in the Southern Ocean is mainly coupled to local climate change. Biogenic opal is an important nutrient that fuels biological production in the surface waters around Antarctica. Recent investigations (Pondaven *et al.* 2000; Chase *et al.* 2003; Bradtmiller *et al.* 2007; Anderson *et al.* 2009) revealed that biogenic opal flux in the Southern Ocean primarily reflects variations in bioproductivity rather than changes in preservation, which enables its use for studying palaeoenvironmental changes during the last glacial cycle. Anderson *et al.* (2009) also identified biogenic opal as an upwelling proxy because, south of the Polar Frontal Zone in the Southern Ocean, its production is ultimately limited by the supply of dissolved Si from the deep ocean. Horn *et al.* (2011) argued that biogenic opal flux might not be a direct upwelling proxy, but could also indicate major changes in nutrient demand such as iron. Until now, high-resolution and continuous biogenic opal flux records from the Southern Ocean extending back to the last interglacial are rare (e.g. Anderson *et al.* 2009) and therefore only limited knowledge exists on how Southern Ocean bioproductivity changed in the past.

We studied two deep-sea cores from the Scotia Sea, with linear sedimentation rates of up to 1.2 m

From: HAMBREY, M. J., BARKER, P. F., BARRETT, P. J., BOWMAN, V., DAVIES, B., SMELLIE, J. L. & TRANTER, M. (eds) 2013. *Antarctic Palaeoenvironments and Earth-Surface Processes*. Geological Society, London, Special Publications, **381**, 245–261. First published online July 30, 2013, http://dx.doi.org/10.1144/SP381.17
© The Geological Society of London 2013. Publishing disclaimer: www.geolsoc.org.uk/pub_ethics

kyr^{-1} (MD07-3134) and 1.8 m kyr^{-1} (MD07-3133). As biogenic opal analysis using the leaching method by Müller & Schneider (1993) is very time-consuming and expensive, we additionally tested several biogenic opal estimation methods, for example Si/Ti-count ratio, wet bulk density, colour b^* and Fourier transform infrared spectroscopy (FTIRS), and compared the results with conventionally measured biogenic opal. FTIRS has been successfully used to determine biogenic opal quantitatively in lacustrine sediment (Vogel *et al.* 2008). We present one of the first studies to assess biogenic opal from FTIRS in marine sediment. Our goal is to provide a high-resolution biogenic opal accumulation rate record, giving the opportunity to study bioproductivity changes at decadal-scale resolution in the Southern Ocean over the last glacial cycle (92.5 ka to present; note that all ages mentioned are calendar ages).

Core material

Sediment cores used in this study originate from the central Scotia Sea (Fig. 1) and were drilled with a Calypso II piston corer during the Marion Dufresne (MD) II cruise 160 in March 2007. Core sites MD07-3133 (57°26′S, 43°27′W, 3101 m water depth, 32.8 m core recovery) and MD07-3134 (59°25′S, 41°28′W, 3663 m water depth, 58.2 m core recovery) are located approximately 450 km apart. Both core sites lie below the carbonate compensation depth. Therefore, the core material is virtually free of biogenic carbonate and consists of varying amounts of lithogenic material and biogenic opal. Homogenous, olive grey to yellow diatomaceous oozes were deposited during warm climatic periods (Marine Isotopic Stages (MIS) 5 and 1), grey to blue-grey diatom-bearing mud during cold periods (MIS 4 and 2), and mostly olive-grey diatomaceous mud during MIS 3.

Chronology

The chronology of sites MD07-3133 and MD07-3134 is detailed in Weber *et al.* (2012). It relies on seven ground-truth data points obtained at site MD07-3134. Accordingly, MIS boundaries 5/4 (71 ka), 4/3 (57 ka), 3/2 (29 ka), and 2/1 (14 ka) comply with 46, 38.5, 16.5 and 11 m core depths, respectively. Relative palaeointensity data indicate a significant drop at approximately 24 m in the core that is considered to represent the Laschamp Event (40.4 ± 1.1 ka; Guillou *et al.* 2004). Furthermore, volcanic ashes also rich in ice-rafted detritus (e.g. site MD07-3134 at 8.9, 13.36, 34.17, and 43.88 m core depth) have been dated and correlated across the Southern Atlantic as layers SA0 (*c.* 14–15 ka) to SA6 (*c.* 55 ka) (Kanfoush *et al.* 2000;

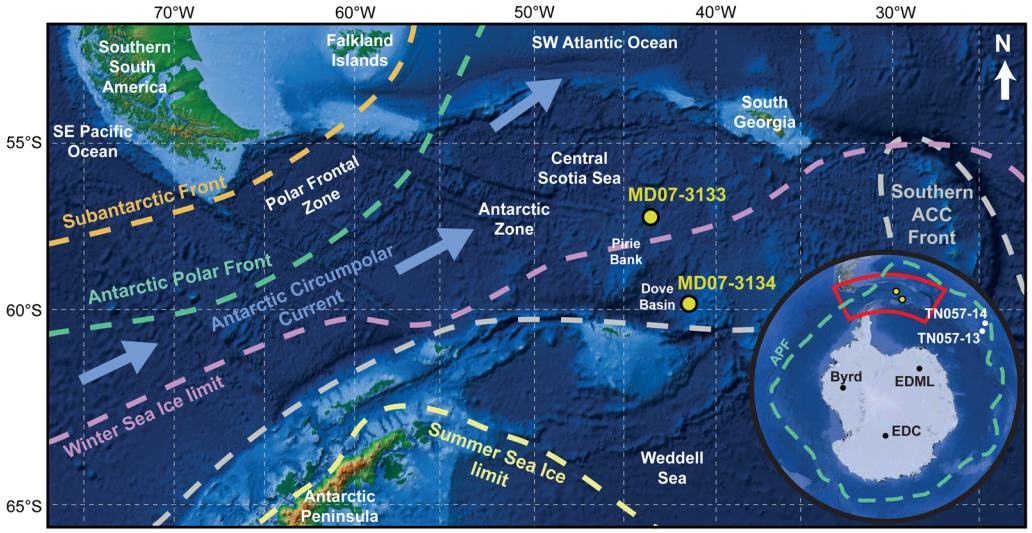

Colour online/ colour hardcopy

Fig. 1. Location map showing the MD07-3133 and MD07-3134 core sites referred to in this study; Subantarctic Front, Antarctic Polar Front, Southern Antarctic Circumpolar Current Front, limits modified from Gersonde *et al.* (2005). Additionally, the positions of Winter and Summer Sea Ice limits today (Gersonde *et al.* 2005; Allen *et al.* 2011) are shown. Also, the direction of Antarctic Circumpolar Current is highlighted. Underlying map originates from http://maps.ngdc.noaa.gov/viewers/bathymetry/ (access date: 20 October 2011). TN core sites are from Anderson *et al.* (2009); Byrd (Ahn & Brook 2008), EPICA Dronning Maud Land (EDML; EPICA Community Members 2006) and EPICA Dome C (EDC; EPICA Community Members 2004) refer to Antarctic ice cores (for details see text).

Nielsen *et al.* 2007). For site MD07-3134, volcanic layers SA0 and SA6 were found at 13.36 and 34.17 m in the core, respectively. The detection of these two layers further supports the independent MIS ground-truth assignation because SA6 is just slightly younger than MIS boundary 4/3, and SA0 is exactly as old as MIS boundary 2/1.

Weber *et al.* (2012) provided convincing arguments that, from the various supply mechanisms proposed for magnetic susceptibility and Ca^{2+} concentrations, that is icebergs, ocean circulation, atmospheric circulation, volcanic sources and sea ice, only atmospheric circulation remains for the Scotia Sea sites. Hence, they correlated both signals to the non-sea-salt Ca^{2+} flux of the European Project for Ice Coring in Antarctica (EPICA) Dronning Maud Land (EDML) record (Fischer *et al.* 2007*a*) to increase the resolution of their age model for site MD07-3134. They applied three stratigraphic approaches to produce a tuned, high-resolution age model, evaluate its quality and provide error estimates: (i) manual picking of tie points; (ii) an automated pattern-matching algorithm; and (iii) a smoothing spline regression using the manual tie points.

As a result, Weber *et al.* (2012) established 48 confident age control points for the last 92.5 kyr. Average linear sedimentation rates are high, ranging from 0.2 to 1.2 m kyr^{-1} and from 0.3 to 1.8 m kyr^{-1} for sites MD07-3134 and MD07-3133, translating into mass accumulation rates (calculated by multiplying linear sedimentation rate with dry bulk densities) of 10–130 and 9–100 g cm^{-2} kyr^{-1}, and into sample resolution of 50–8 years and 33–5 years (given a sample increment of 1 cm), respectively.

Tuning magnetic susceptibility to the non-sea-salt Ca^{2+} flux has significant implications for the quality and reliability of the age model. The fact that the two signals are more or less phase-locked during this procedure is reasonable because dust transport from Patagonia to Antarctica takes only approximately a week (Li *et al.* 2010). Therefore, no major leads or lags should be involved for atmospheric transport. Accordingly, the chronology of our two sites provides a precise and high-resolution age model for Southern Ocean deep-sea sediment.

Setting

The Scotia Sea is located in the Atlantic Sector of the Southern Ocean where the Antarctic Circumpolar Current dominates oceanic circulation. It is the world's largest current with a transport volume of approximately 134 Sverdrup (1 Sv = 10^6 m^3 s^{-1}; Whitworth & Peterson 1985) flowing eastward around the Antarctic continent. The Antarctic Circumpolar Current includes, in most regions, water masses from the seafloor to the surface. Its velocity generally decreases with depth but is also severely influenced by local seabed topography (Pugh *et al.* 2009). Uniquely connecting the Atlantic, Indian and Pacific, the Antarctic Circumpolar Current allows for heat, nutrient and salt exchange between the oceans (Maldonado *et al.* 2003), accordingly playing an important role in global climate control (Pugh *et al.* 2009). It is mainly wind-driven by the Southern Hemisphere Westerlies between 45 and 55°S. These Westerlies are also responsible for transporting surface waters away from Antarctica through Ekman transport, leading to upwelling of mid-depth water (2–3 km) south of the current, a unique process restricted to the Southern Ocean (Berger & Loutre 1991).

In the Scotia Sea, the Antarctic Circumpolar Current flows between the Subtropical Front and the Southern Antarctic Circumpolar Current Front (Fig. 1). Its flow is concentrated in circumpolar, vertically coherent, seafloor-reaching fronts: the Subantarctic Front, the Antarctic Polar Front and the Southern Antarctic Circumpolar Current Front (Orsi *et al.* 1995). The Antarctic Polar Front is the northern limit of wind-driven, nutrient-rich deep-water upwelling because of northward Ekman transport. It therefore forms an ecological and physical water–mass boundary to colder, more silicate-rich and less saline water masses south of it (Pondaven *et al.* 2000; Dezileau *et al.* 2003; Cassar *et al.* 2007; Diekmann 2007), where both core sites are located (Fig. 1). The area between the Antarctic Polar Front and the northern limit of seasonal sea ice is known as the Circum-Antarctic Opal Belt with high biosiliceous production rates (Geibert *et al.* 2005; Diekmann 2007). The southern boundary of siliceous deposits corresponds well to the Southern Antarctic Circumpolar Current Front in the Atlantic Sector of the Southern Ocean (Geibert *et al.* 2005).

Methods

We used a Minolta spectrophotometer CM-2002 to measure L^*, a^* and b^* colour components at 1 cm intervals (Weber 1998). To obtain information on chemical element distribution (e.g. for Si, Ti), every centimetre of sediment was analysed according to the method of Richter *et al.* (2006) using an Avaatech X-ray Fluorescence Core Scanner (Jansen *et al.* 1998).

Sediment physical properties such as wet bulk density and magnetic susceptibility (κ volume specific) were measured non-destructively every centimetre with a Geotek Multi-Sensor Core Logger (Weber *et al.* 1997). Dry bulk densities, which are

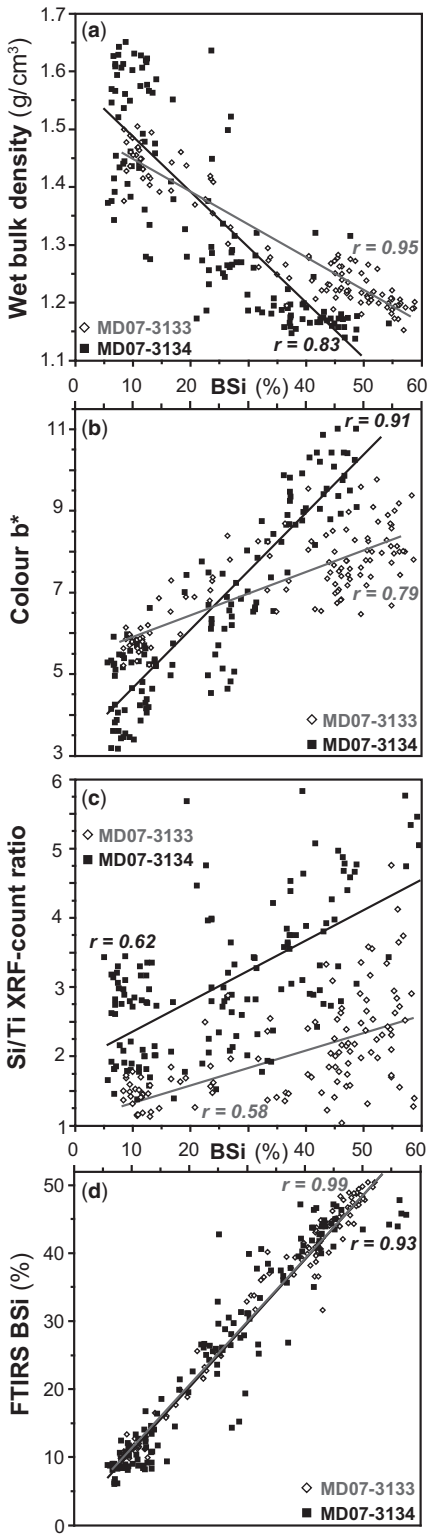

required for the calculation of mass accumulation rates, were calculated from wet bulk densities using an iteration procedure described in Weber *et al.* (1997), by applying specific mass attenuation coefficients to each measurement to account for fluctuating water content and grain density. To check its accuracy we also compared the non-destructive data with dry bulk densities determined on freeze-dried samples.

In addition to measuring biogenic opal on specific samples we implemented several strategies to estimate it at high spatial resolution. We first analysed biogenic opal by leaching the sediment in 1 M NaOH-solution according to the method of Müller & Schneider (1993). The initial values for biogenic silicon were corrected by adding 10 wt% H_2O for the water bound in the amorphous opal skeleton (biogenic opal = biogenic $opal_{M\&S}$ + 10% H_2O). All resulting data needed to be corrected for the sea salt content of the pore fluid (35‰). As this leaching method is relatively expensive and time-consuming, measurements were restricted to 10 cm intervals of specific sections that exhibit large-amplitude variations (MD07-3133: 1655–2785 cm, 112 samples; MD07-3134: 745–1785 cm, 4135–4585 cm, 141 samples).

Biogenic opal-rich, unconsolidated sediments exhibit extremely high porosities because interstitial fluid rests both within the shells (intragranular) and in the pore space (intergranular). The high sediment water contents as well as the lower grain densities of biogenic opal, in contrast to detrital material and biogenic carbonate, cause the extremely low wet and dry bulk densities of biogenic opal-rich sediments. Therefore, wet bulk densities are negatively correlated to biogenic opal (Weber 1998) for diatom-rich deep-sea sediments well below the carbonate compensation depth, and hence biogenic opal can be estimated from wet bulk densities using linear correlation coefficients (Fig. 2a).

Another striking correlation is given for colour b^* and biogenic opal in diatom-rich sediment (Weber 1998), that is, the more yellow the sediment, the higher the amount of biogenic opal, whereas more bluish colours indicate low biogenic opal. Accordingly, we derived linear correlation coefficients to estimate the amount of biogenic

Fig. 2. Scatter plots illustrating linear correlations for conventionally leached biogenic opal (BSi) values (method see Müller & Schneider 1993) and BSi content estimated from wet bulk density (**a**), colour b^* (**b**), XRF-core-scanner measured Si/Ti-count ratio (**c**) and Fourier transform infrared spectroscopy (FTIRS) (**d**; method see Rosén *et al.* 2010). White diamonds and grey lines refer to site MD07-3133; black squares and black lines indicate data from site MD07-3134.

opal from colour b^* for Scotia Sea sites MD07-3133 and MD07-3134 (Fig. 2b).

Also, we used the ratio of Si and Ti XRF-counts to obtain information on biogenic opal changes. Si originates from either detrital siliciclastics or biogenic, mostly diatom sources. Because Ti reflects only clastic input (Murray *et al.* 1993), the XRF Si/Ti ratio should only represent changes in biogenic opal (Francus *et al.* 2009; Balascio *et al.* 2011). Because XRF core-scanner measurements were made at higher resolution than some other proxies (1 cm increments), we implemented a nine-point moving average to smooth the data (using AnalySeries 2.0.4.2.; Paillard *et al.* 1996). Then we used the linear correlation between the Si/Ti XRF-count ratio and leached biogenic opal to calculate biogenic opal values, depending on Si/Ti-count ratios (Fig. 2c).

Furthermore, we implemented FTIRS to obtain high-resolution information on biogenic opal and other biogeochemical sediment components. FTIRS is a fast and relatively inexpensive technique, which requires only 11 mg of sample material (Rosén *et al.* 2011). It was therefore employed at 10 cm intervals over the entire core lengths of sites MD07-3133 and MD07-3134 (316 and 575 samples, respectively) at the Climate Impacts Research Centre in Umeå, Sweden. FTIRS has been successfully used to determine, quantitatively, total inorganic and organic carbon, and biogenic opal in lacustrine sediment (Vogel *et al.* 2008). Here, we present one of the first studies to assess these sediment properties quantitatively for marine sediment. Samples were first freeze-dried and ground to <63 μm using a swing mill. In addition, 500 mg of oven-dried (80 °C) potassium bromide (KBr, Merck), which is transparent in the infrared band, was added to each sample. This is necessary to avoid very high absorbances (>2), which are released by low intensities of infrared light that would otherwise reach the detector and produce higher noise levels in the data and spectral distortions (Griffiths & De Haseth 1986). The samples were measured using an FTIR spectrometer (Bruker Vertex 70) equipped with a diffuse reflectance accessory. Each sample was scanned 128 times and data were collected every 2 cm^{-1} (reciprocal centimetres). The measurement resolution was 4 cm^{-1} for wavenumbers between 3750 and 400 cm^{-1}, which equals wavelengths from 2666 to 25 000 nm, thus yielding 1735 data points per sample. To avoid variations caused by temperature, all samples were placed in the same temperature-controlled laboratory (25 $\pm$ 0.2 °C) as the FTIRS device for at least 5 h prior to analysis. Multiple scatter correction and baseline correction were used to linearize spectra and remove variation in spectra caused by noise (Geladi *et al.* 1985; Rosén *et al.* 2010). Baseline correction performs a linear correction of the spectra so that two points (3750 and 2210–2200 cm^{-1}) equal zero. Multiple scatter correction removes spectral variation arising from different effective path lengths and particle sizes (Geladi *et al.* 1985). Partial least squares regression was used to develop quantitative calibration models between FTIR spectra of sediment and conventionally measured sediment properties (Martens & Naes 1989). An internal calibration model based on 253 samples from MD07-3133 and MD07-3134 was regressed on 253 conventionally determined sea salt corrected mass percentage biogenic opal contents using the leaching technique (Müller & Schneider 1993; Vogel *et al.* 2008). Wavenumbers between 450 and 1320 cm^{-1} were used in the partial least squares regression model, that is, a region where different types of silicates absorb. Although different silicates absorb in the FTIRS wavenumber region between 1050 and 1250 cm^{-1}, it is not necessary to subtract spectra as the curve's shape shows characteristic differences for, for example, quartz and biogenic opal. The predictive performance of the partial least squares regression calibration model was assessed by 10% cross-validation. This means that the calibration model was developed using 90% of data of the calibration samples with the remaining 10% used to test the predictions. This process was repeated a total of 10 times as each group, in turn, was set aside. Root mean squared error of cross-validation was used as an estimate of prediction error. All primary sediment properties were square root transformed prior to the analysis. SIMCA-P 11.5 (Umetrics AB, SE-907 19 Umeå, Sweden) was used for all multivariate data analyses.

Correction of sediment focusing using $^{230}Th_{xs}$ normalization

The extremely high sedimentation rates of up to 1.8 m kyr^{-1} clearly indicate that the sediments of this site have been subject to massive sediment focusing induced by bottom currents. This is observed at many locations in the Southern Ocean and results in completely erroneous mass accumulation rates, which can be off by a factor of 12 (Frank *et al.* 1999) or even more (this study). For the calculation of realistic mass accumulation rates (rain rates) of biogenic opal and other components, the effects of sediment focusing have to be quantified and be corrected for applying excess ^{230}Th ($^{230}Th_{xs}$) normalization (Kumar *et al.* 1995; Frank *et al.* 1996, 2000; Francois *et al.* 2004). This method is based on the constant production of ^{230}Th from its global homogenously distributed radioactive parent ^{234}U. In contrast to U, Th is

highly particle reactive, resulting in essentially the entire amount of locally produced ^{230}Th being deposited in the sediments below. This means that the mass accumulation rate of ^{230}Th in the sediments should match its production in the overlying water column. Given that ^{230}Th can only be advectively transported in solution over very short distances as a consequence of its particle reactivity, any significant increases over the expected ^{230}Th-mass accumulation rate must be a result of sediment focusing and can be quantitatively corrected for by relating it to the expected flux at any particular location.

For the determination of the activities of ^{230}Th, ^{232}Th, ^{234}U and ^{238}U, between 50 and 90 mg of sediment were weighed and spiked with ^{229}Th/^{233}U/^{236}U in the laboratory of GEOMAR in Kiel. The samples were first treated with aqua regia and were then subjected to total dissolution in a mixture of concentrated nitric, hydrofluoric and perchloric acid. Subsequently U and Th were separated from each other and from disturbing matrix elements via ion exchange chromatography using a Uteva resin (Eichrom). The activities of the U and Th isotopes were determined on an Agilent 7500 quadrupole mass spectrometer. The precision of the measurements was better than 1% (2 standard errors) for the respective U isotopes and better than 2% (2 standard errors) for the Th isotopes. For the calculation of $^{230}Th_{xs}$ activities see Frank *et al.* (1996).

Results

Correlation coefficients of $r = 0.95$ and 0.83 indicate that wet bulk density changes at sites MD07-3133 and MD07-3134 are mainly caused by fluctuations in biogenic opal content (Fig. 2a). Also colour b^* changes predominantly reflect fluctuations in biogenic opal content (Fig. 2b), although their relation is, with correlation coefficients of $r = 0.91$ and 0.79, not as striking as for wet bulk density. The generally good correlation coefficients (≥ 0.79) let us assume that both wet bulk density and colour b^* can be used to estimate realistic biogenic opal contents (within the given errors).

Additionally, XRF-measured Si/Ti-count ratios provide, to some extent, rough information about biogenic opal fluctuations. The correlation coefficient for Si/Ti and biogenic opal is $r = 0.58$ and 0.62 for sites MD07-3133 and MD07-3134 (Fig. 2c). However, its use as a biogenic opal proxy is questionable owing to uncertainties associated with Ti values (see Discussion for further explanation).

The most promising estimation method is FTIRS (Fig. 2d) with correlation coefficients of $r = 0.99$ and $r = 0.93$ for sites MD07-3133 and MD07-3134. The models of leached and FTIRS-estimated biogenic opal show good statistical performance, with cross-validated root mean squared errors of 4.8% (MD07-3133), respectively 8.7% (MD07-3134) of the gradient. FTIRS provides the closest similarities of all estimation methods to the reference method of conventional leaching.

We then calculated biogenic opal contents from the various proxy data sets for sites MD07-3133 and MD07-3134 (Fig. 3), using the linear regression lines discussed above (Fig. 2). In general, the same overall trend is recognizable for all biogenic opal estimation curves; however, the amplitude varies significantly for some parts of the cores. Higher linear sedimentation rates lead to higher-resolution data for site MD07-3133 relative to site MD07-3134, specifically for the Holocene section. However, both cores share the same overall trend and principal features. As expected from the correlation coefficients, FTIRS-estimated and leached biogenic opal share the most commonalities. Biogenic opal contents estimated from colour b^* capture the glacial to interglacial transition; however, colour b^* overestimates biogenic opal contents for the uppermost and lowermost core sections of site MD07-3133. In fact, for the upper 12 m of MD07-3133, estimates from colour b^*, wet bulk density and the Si/Ti-count ratio show substantial discrepancies relative to FTIRS estimates (Fig. 3).

On average, the highest biogenic opal contents occur during interglacial MIS 5 and 1, confirming results of earlier studies on deep-sea sediment in the Atlantic sector (e.g. Charles *et al.* 1991; Mortlock *et al.* 1991; Pudsey & Howe 1998; Diekmann 2007), the Indian Sector (Bareille *et al.* 1998) and the Pacific Sector (Chase *et al.* 2003) of the Southern Ocean, south of the Antarctic Polar Front. Interglacial MIS 3 shows intermediate contents of biogenic opal with an overall decreasing trend towards MIS 2. During glacials MIS 4 and 2, absolute minima in biogenic opal contents are noticeable (Fig. 3). Surprisingly, maximum biogenic opal contents occur during glacial MIS 4 (site MD07-3134). These extraordinary high values seem robust (i.e. not caused by analytical errors), as five data points scatter around 60% biogenic opal in less than 1 m of sediment core. This section also shows low densities and yellower sediment colour, corresponding to substantially elevated biogenic opal contents. FTIRS also indicates high biogenic opal values for this section, whereas the highest FTIRS-estimated biogenic opal values (*c.* 67%) occur at the end of MIS 5. MIS 5 and 4 show high-amplitude and high-frequency changes in biogenic opal, whereas during MIS 2 and 1 biogenic opal contents were relatively stable, showing only low-amplitude fluctuations.

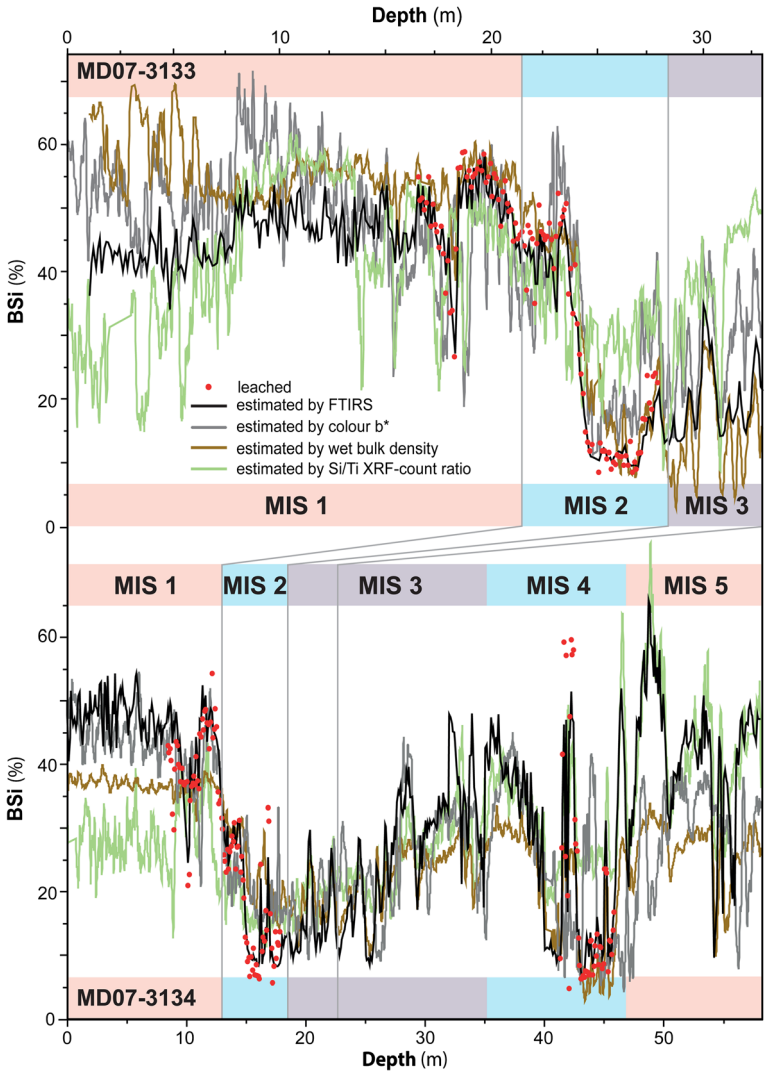

Colour online/ colour hardcopy

Fig. 3. Comparison of biogenic opal (BSi) contents evaluated with different methods for sites MD07-3133 (top) and MD07-3134 (bottom): conventionally (leached; data points highlighted as red dots; method see Müller & Schneider 1993); and BSi estimated from wet bulk density (brown curve), colour *b** (grey curve), Fourier transform infrared spectroscopy (FTIRS; black curve; method see Rosén *et al.* 2010) and XRF-core-scanner measured Si/Ti-count ratio (green curve; method see Balascio *et al.* 2011). Marine Isotopic Stages (MIS) 1–5 are plotted for reference (Lisiecki & Raymo 2005).

To better understand the biogenic opal sedimentation changes through time, we calculated mass accumulation rates for FTIRS-estimated biogenic opal contents (Fig. 4e), which we consider the most precise estimation method (see Methods; Fig. 2). This was done by multiplying the biogenic opal content as a percentage by the mass accumulation rate, that is, the product of sedimentation rate and dry bulk density (Fig. 4a, b). Instead of linear sedimentation rates, we used sedimentation rates estimated from a cubic smoothing spline age-model (Weber *et al.* 2012; Fig. 4a, grey lines). This overcomes the problems of normal splines, which do not include errors and so might produce outliers and artefacts, hence, representing more realistic sedimentation rates. Both cores exhibit extremely high sedimentation rates in some sections with values up to 1.8 and 1.2 m kyr^{-1} for sites MD07-3133 and MD07-3134. Warmer periods (MIS 3 and 1) show approximately 1.5–2 times

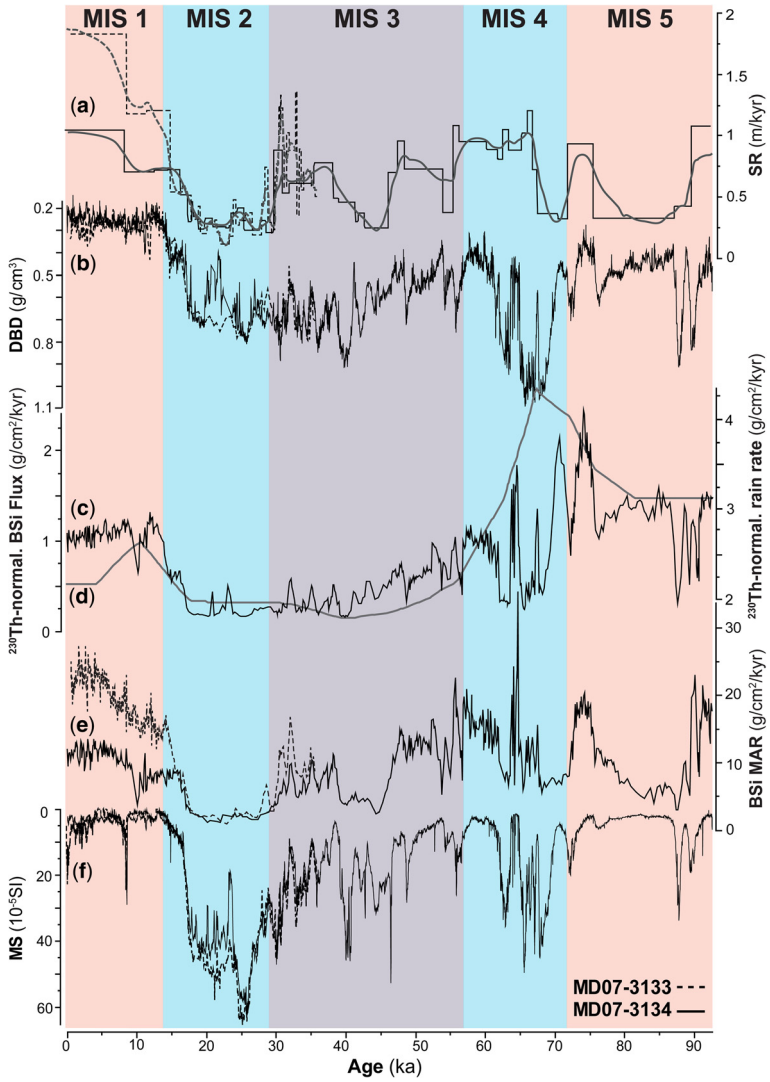

Fig. 4. Sites MD07-3133 (dashed lines) and MD07-3134 (solid lines) records: (**a**) Linear sedimentation rate (LSR) (black lines) and sedimentation rates (SR) estimated from a cubic smoothing spline age-model (grey lines; Weber *et al.* 2012). (**b**) Dry bulk density (DBD). (**c**) ^{230}Th-normalized biogenic opal (BSi) flux evaluated using the FTIRS estimated biogenic opal values (for method see Rosén *et al.* 2010). (**d**) ^{230}Th-normalized average rain rate. (**e**) BSi mass accumulation rate (MAR) evaluated using FTIRS estimated BSi values multiplied by SR from a cubic smoothing spline age-model (a) and DBD (b). (**f**) Magnetic susceptibility (MS) records as dust proxy (Weber *et al.* 2012). MIS 1–5 are plotted for reference (Lisiecki & Raymo 2005).

Colour online/ mono hardcopy

increased sedimentation rates at sites MD07-3133 relative to site MD07-3134, whereas during MIS 2 nearly identical rates occur at both core sites (Fig. 4a). The sedimentation rates and biogenic opal mass accumulation rates show a relatively complicated glacial-to-interglacial pattern with large-amplitude changes. While the biogenic opal mass accumulation rate reaches its minimum during the Last Glacial Maximum with values of approximately 3 g cm^{-2} kyr^{-1} at both core sites, up to 10 times higher rates are observed during MIS 4 (Fig. 4e).

^{230}Th-normalization data for MD07-3134 show that sediment focusing was very high, ranging from 5 (minimum value at 84.3 ka) to 29 (maximum value at 55.9 ka). During the interglacials

the focusing factor ranged between 5 and 13, meaning that 5–13 times more sediment was added laterally to the core site via focusing than vertically through the water column. In the last glacial, in particular MIS 3, the focusing factors were generally even higher and ranged between 11 and 29. Strictly speaking, the ^{230}Th-normalized fluxes can only be applied for the 10 samples on which ^{230}Th was measured because there is no control over changes in sediment focusing between the depths of the measured ^{230}Th-normalized values. We are aware of this limitation and the interpolated ^{230}Th-normalized rain rates are just provided as an approximation for illustrative purposes until we have additional ^{230}Th-normalized data.

The interpolated rain rate for MD07-3134 (Fig. 4d) varies between 2 and 4.3 g cm^{-2} kyr^{-1}, with maximum values around 67 ka resulting from intermediate dry bulk densities (Fig. 4b), a focusing factor of 10 and a relatively high linear sedimentation rate (Fig. 4a). In order to achieve a more realistic record of the biogenic opal flux we multiplied ^{230}Th-normalized rain rates and FTIRS-estimated biogenic opal amount to get ^{230}Th-normalized biogenic opal flux (Fig. 4c). The calculated ^{230}Th-normalized biogenic opal flux varies from 0.2 to 2.5 g cm^{-2} kyr^{-1}. Maxima occur during interglacials, with mean values of 1 (MIS 1) and 1.4 (MIS 5) g cm^{-2} kyr^{-1}, whereas glacial MIS 2 and 3 were generally characterized by lower values near 0.5 g cm^{-2} kyr^{-1}. MIS 4 shows large short-term fluctuations, which, however, would need to be confirmed by additional ^{230}Th$_{xs}$ measurements at higher resolution. In general, the ^{230}Th-normalized biogenic opal flux data (Fig. 4c) show a similar pattern over the past 92.5 kyr compared with the uncorrected biogenic opal accumulation rates (Fig. 4d) albeit with realistic numbers when compared with other sites in the Atlantic sector of the Southern Ocean (Kumar *et al.* 1995; Frank *et al.* 2000). As we have no ^{230}Th-normalization data for MD07-3133, we can only suggest that the sediment focusing was analogous and maybe even higher than at the MD07-3134 core site, as the linear sedimentation rate shows a similar trend, but higher values (Fig. 4a).

Discussion

To what extent are biogenic opal estimation methods reliable?

Biogenic opal can be analysed and estimated using various techniques, but no standardized determination methodology exists because each method has advantages and drawbacks. As deduced from Figure 3, the main biogenic opal fluctuations are captured by all estimation methods, so all methods can be used to decipher general biogenic opal trends; however, there are some strong discrepancies. Leaching according to Müller & Schneider (1993) is one of the most commonly used methods because of its simplicity and robustness (Swann 2010). However, samples with $\leq$10% biogenic opal might be affected by the pH value of the leaching solution (Schlüter & Rickert 1998).

XRF Si/Ti ratio is often used to indicate biogenic opal content changes in sediments (e.g. Francus *et al.* 2009; Balascio *et al.* 2011; Johnson *et al.* 2011). Nonetheless, Tjallingii *et al.* (2007) found reduced XRF-element intensities for light elements such as Si and Al of wet material relative to dried material, which they relate to differences in water contents. Accordingly, this can lead to misinterpretations of wet-measured samples. Our Si/Ti-count ratios reflect roughly the main biogenic opal fluctuations, especially at MD07-3134 (Fig. 3), but they should be only seen as rough estimations because of the given measurement uncertainties. Colour b^* can also be a useful parameter to estimate biogenic opal content of carbonate-free sediments that mainly contain varying amounts of biogenic opal, quartz and clay minerals. Our estimation shows that wet bulk density is also useful to roughly estimate biogenic opal content. It would also yield reliable results for sediments containing biogenic carbonate because biogenic opal has significantly lower densities (*c.* 2.2 g cm^{-3}) than biogenic carbonate (*c.* 2.8 g cm^{-3}) or detrital material (*c.* 2.6 g cm^{-3}). However, greater amounts of organic carbon (density of *c.* 1.4 g cm^{-3}) would lead to misinterpretations (Weber 1998).

Estimates from colour b^*, wet bulk density and the Si/Ti-count ratio for the upper 12 m of MD07-3133 show substantial discrepancies relative to FTIRS estimates (Fig. 3). This may be due to a combination of coring effect and sediment facies, that is, the upper parts of core MD07-3133 were partially supersaturated with water. These sections leaked pore water when they were cut into 1 m sections because of missing cohesive forces typical for the fabric of diatomaceous oozes. Accordingly, scanning techniques such as the Multi-Sensor Core Logger and the XRF-scanner measured false values in the uppermost core section, because they rely on completely filled core liners as well as smooth and even surfaces. So these estimations have limitations if sediments are supersaturated with water or show uneven surfaces.

A number of studies (e.g. Vogel *et al.* 2008; Rosén *et al.* 2011) show that FTIRS can be used to gain high-resolution and high-quality geochemical information on lacustrine sediment consisting of varying amounts of inorganic and organic components. Our results (Figs 2d & 3) also indicate

that FTIRS is a very promising and useful tool for studying marine sediment composition. Correlation coefficients of $r = 0.99$ (MD07-3133) and $r = 0.93$ (MD07-3134) and an all-gradient accordance (Fig. 2d) underline our suggestion that FTIRS seems to be the most reliable estimation method, and hence can be used successfully for deep-sea sediment analysis. Therefore, we used the FTIRS results for all further discussions and comparisons (Figs 4 & 5).

Biogenic opal flux as a bioproductivity proxy

There is a strong debate on the reliability of biogenic opal flux data for indicating bioproductivity. It is still not entirely clear whether biogenic opal preservation is consistent over longer time periods and how the silicon cycle is coupled with the carbon biogeochemical cycle during interglacials (e.g. Pondaven *et al.* 2000; Ragueneau *et al.* 2000; Dezileau *et al.* 2003). However, in recent years, a number of studies indicate that biogenic opal flux can be used as bioproductivity proxy. Chase *et al.* (2003) and Bradtmiller *et al.* (2007) argued that biogenic opal flux reflects variations in diatom productivity and not changes in biogenic opal preservation. For the Indian sector Pondaven *et al.* (2000) found that local differences in biogenic opal preservation, apparent in the polar frontal zone and south of it, have a modulating but no primary effect on biogenic opal flux fluctuations. The good correlation of site MD07-3133 and MD07-3134 biogenic opal mass accumulation rate records (Fig. 5e), which are approximately 450 km apart (Fig. 1), indicates that this argument is also true for the central Scotia Sea.

Presently, the $^{231}Pa/^{230}Th$ ratio is the most accurate and most commonly used proxy for analysing particle and water mass transport in the Southern Ocean, for example, past opal fluxes (Kretschmer *et al.* 2011). Also Anderson *et al.* (2009) found strong correlation between the biogenic opal flux (i.e. mass accumulation rate) and $^{231}Pa/^{230}Th$ ratios, which are not altered by biogenic material loss during early diagenesis (Chase *et al.* 2003) in Southern Ocean sediment. This led them to the conclusion that biogenic opal flux variations reflect changes in biogenic opal production and silicon supply, rather than changes in preservation.

Estimated mean sedimentation rates are extremely high at both core sites: the mean linear sedimentation rate for MIS 1 is 0.9 (MD07-3134) and 1.6 (MD07-3133) m kyr^{-1}; it is approximately 0.5 m kyr^{-1} (MD07-3133 and MD07-3134) for MIS 2, 0.7 m kyr^{-1} (MD07-3134) for MIS 3 as well as MIS 5, and 0.9 m kyr^{-1} (MD07-3134) for MIS 4. Our values are more than 10–30 times higher than reported in previous studies, where rates of less than 5 cm kyr^{-1} for interglacials, and more than 5 cm kyr^{-1} for glacial times in the Scotia Sea were estimated (Pudsey & Howe 1998; Diekmann *et al.* 2000; Pugh *et al.* 2009). Accordingly, we conclude that both core sites are strongly influenced by sediment focusing, which is also reflected in the ^{230}Th normalized data of MD07-3134 (Fig. 4c, d), showing quite strong variability in sediment focusing with average interglacial values of 8 and average glacial values of 20. To our knowledge, these are some of the highest focusing factors ever determined with this method. The calculated ^{230}Th normalized rain rates (Fig. 4d) now correspond very well to other Southern Ocean sites, for instance, neighbouring core PS2319-1 (Francois *et al.* 2004). However, the ^{230}Th normalized biogenic opal flux overall shows the same trend as our estimated biogenic opal mass accumulation rate (Fig. 4e) for MD07-3134.

High sediment focusing of course is an indicator for bottom currents affecting an area, but these currents obviously did not vary so dynamically that they destroyed the dust-related signal (Pugh *et al.* 2009; Weber *et al.* 2012) within the decadal resolution. In contrast they collected the sediments from an upstream mostly shallower region and focused the material deposition to the core sites, thereby enhancing time resolution of the sedimentary record. By increasing the focusing factor from 8 to 20 during glacials, this sediment advection acted like a slow motion frame. The Antarctic Circumpolar Current has a significant effect on seafloor sedimentation in that area (Pudsey & Howe 1998). As a mainly wind-driven current (Maldonado *et al.* 2003) we assume that it resulted in decadal and centennial variations, which are comparable to dust climate signals, for example, Antarctic EDML non-sea-salt Ca^{2+} flux (Fischer *et al.* 2007*a*).

In regions such as the Antarctic Zone, where nutrient concentration is constantly high, iron availability strongly influences bioproductivity (Martínez-Garcia *et al.* 2011). Different iron fertilization experiments (e.g. Martin *et al.* 1990; Boyd *et al.* 2000) showed that Southern Ocean productivity is limited by Fe-deficiency. Coastal sediments, aerosols, upwelling, ice melting and vertical mixing can supply iron to the Southern Ocean (Cassar *et al.* 2007); however, today the major nutrient and iron supply originates from upwelling water masses or lateral advection (Meskhidze *et al.* 2007; Martínez-Garcia *et al.* 2011). The influence of dust-transported aeolian iron on bioproductivity is still debated. Erickson *et al.* (2003) suggested that bioproductivity in the Antarctic Circumpolar Current region is mainly controlled by atmospheric dust-Fe, mostly from Patagonia, whereas Kaufmann *et al.* (2010) argued that dust flux variations had no major influence on

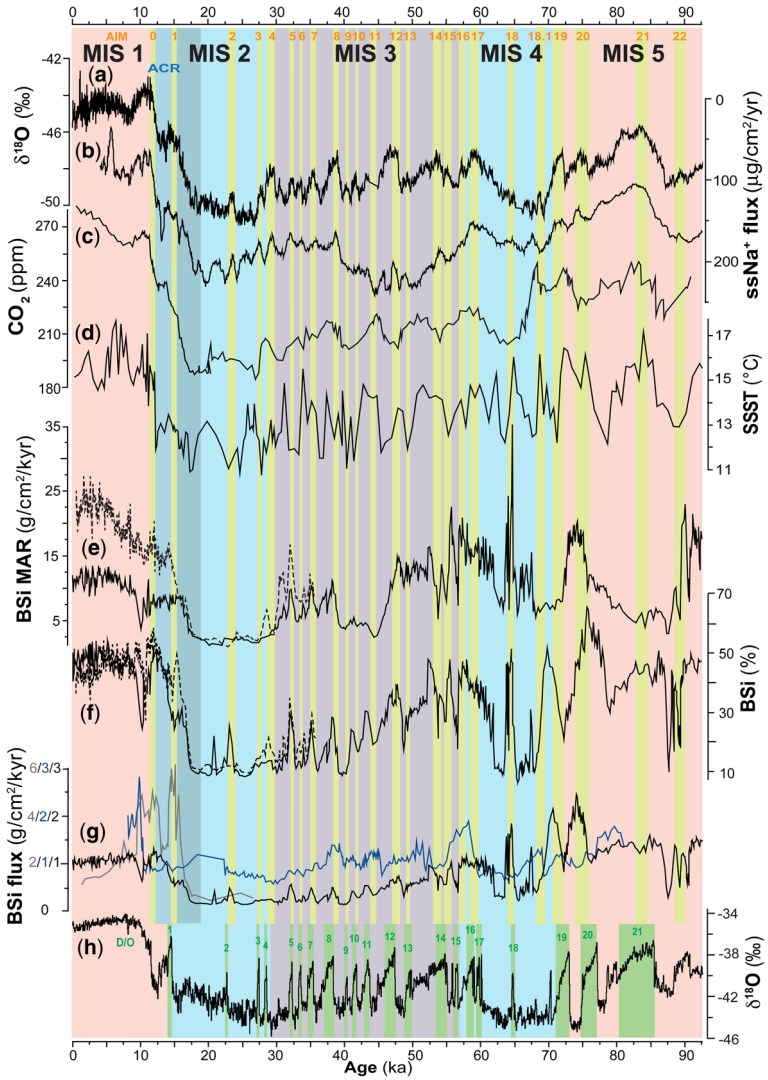

Fig. 5. Palaeoclimate and palaeoproductivity records for the last 92.5 kyr highlighting millennial-scale climate fluctuations during the last glacial: (**a** and **b**) EDML ice core $\delta^{18}O$ (EPICA Community Members 2006) as local ice sheet temperature indicator and sea-salt Na^{+} flux (Fischer *et al.* 2007*a*) as sea ice proxy; (**c**) combined record of CO_2 measured at EDC (0–20 ka; Monnin 2006) and Byrd ice core (20–91 ka; Ahn & Brook 2008); (**d**) radiolarian-based summer sea-surface temperature (SSST) reconstruction derived at ODP site 1089 (Cortese & Abelmann 2002) in the Atlantic sector of the Southern Ocean; (**e**) biogenic opal mass accumulation rates (BSi MAR) for MD07-3133 (dashed line) and MD07-3134 (solid line) core sites calculated from multiplying FTIRS-estimated BSi (method see Rosén *et al.* 2010) by dry bulk density and sedimentation rates estimated from a cubic smoothing spline age-model (Weber *et al.* 2012); (**f**) MD07-3133 and MD07-3134 BSi content as percentages estimated with FTIRS; (**g**) ^{230}Th-normalized BSi flux from sediment cores MD07-3134 (black line), TN057-13PC (grey line) and TN057-14PC (blue line; Anderson *et al.* 2009) from the SE Atlantic Sector of the Southern Ocean (Fig. 1); (**h**) is Northern Hemisphere NGRIP ice core $\delta^{18}O$ (NGRIP Members 2004). MIS 1–5 are plotted for reference (Lisiecki & Raymo 2005), as well as Antarctic Isotopic Maxima (EPICA Community Members 2006; Stenni *et al.* 2010), Antarctic Cold Reversal (Rahmstorf 2002) and Daansgard–Oeschger–Cycles (Blunier & Brook 2001).

Colour online/ colour hardcopy

Southern Ocean productivity over the last 150 kyr. Further, modelling studies suggest that upwelling delivers approximately 99% of micronutrients to the Southern Ocean rather than dust (Lefèvre & Watson 1999). At sites MD07-3133 and MD07-3134 dust-indicator magnetic susceptibility

exhibits mostly minima when biogenic opal mass accumulation rate is high and vice versa (Fig. 4e, f). During the Last Glacial Maximum, dust transport was significantly intensified and led to 10–30 times higher concentrations in Antarctic ice cores (Delmonte *et al.* 2004) and in the Scotia Sea (sites MD07-3133 and MD07-3134; Weber *et al.* 2012), whereas biogenic opal mass accumulation rates were extremely low during that period. Accordingly, we believe that iron-fertilization via dust transport is not the main driver of bioproductivity changes in the Scotia Sea. In addition, iron released from melting icebergs (Raiswell 2011), that is, Fe either from terrigenous material or aeolian dust (Lin *et al.* 2011), might have a minor affect on bioproductivity, as both sediment core sites are within the so-called 'iceberg alley' (Anderson & Andrews 1999; Stuart & Long 2011).

Biogenic opal export increase at the end of the last glacial could reflect higher nutrient content in upwelling waters or just intensified upwelling, more fractional utilization of nutrients or, to a lesser extent, better preservation of sinking biogenic opal (Horn *et al.* 2011). Allen *et al.* (2011) conclude that reduced surface water productivity and/or export in the Scotia Sea during the Last Glacial Maximum, caused by enhanced sea ice cover, lower sea surface temperatures and therefore shorter growing seasons, and not changes in dissolution processes, are more likely to explain the lower abundance of diatoms in sediment cores during the Last Glacial Maximum.

Bioproductivity changes since the last interglacial

Given the above arguments, we believe that the Scotia Sea biogenic opal mass accumulation rates at sites MD07-3133 and MD07-3134 mainly provide records of changing bioproductivity since the last interglacial. Interestingly, a relatively complicated glacial-to-interglacial pattern is noticeable (Fig. 5e–g). Large-amplitude millennial-scale fluctuations occur in the Scotia Sea records, which exhibit decadal-scale sample resolution. We estimate the lowest bioproductivity for the Last Glacial Maximum, while Southern Hemisphere Westerlies seem to have been located approximately 7–10° latitude north of their present position (e.g. Moreno *et al.* 1999; Toggweiler *et al.* 2006). During that time upwelling of silica- and CO_2-rich, relatively warm mid-depth water to the sea surface was reduced significantly – approximately 30% relative to today (Horn *et al.* 2011) – which led to low-temperature and low-salinity surface waters that supported sea ice formation in the Southern Ocean (Toggweiler *et al.* 2006). Also, micronutrient availability in the Scotia Sea was at a minimum during the Last Glacial Maximum (Hendry *et al.* 2011). As shown in Figure 5, low biogenic opal mass accumulation rates at the Last Glacial Maximum correspond to (i) low $\delta^{18}O$ values of the EDML ice core (Fig. 5a), which provide a local ice sheet temperature indicator (EPICA Community Members 2006) and (ii) high sea-salt Na^+ fluxes of the EDML ice core (Fig. 5b; Fischer *et al.* 2007*b*), which reflect intense sea ice cover. During MIS 2, decreased biogenic opal mass accumulation rates were estimated by Diekmann (2007) for the southern parts of Antarctic Circumpolar Current in all Southern Ocean sectors. Also Frank *et al.* (2000), Chase *et al.* (2003), Dezileau *et al.* (2003) and Bradtmiller *et al.* (2009) found lower biogenic opal accumulation rates south of the Antarctic Polar Front during MIS 2 relative to MIS 1, thereby suggesting less diatom productivity during MIS 2.

Around 17 ka, atmospheric CO_2 increased rapidly and the Southern Hemisphere Westerlies probably shifted south (Toggweiler 2009). It remains unclear whether the shift in Southern Hemisphere Westerlies caused the rise in CO_2 or if the shift was a result of rising CO_2. Denton *et al.* (2010) show that reorganization of ocean circulation, induced by intensified cooling as a result of large meltwater pulses in the Northern Hemisphere, weakened the Atlantic Meridional Overturning Circulation. This consequently led to a poleward shift of the Southern Hemisphere Westerlies, intensified upwelling of CO_2-rich mid-depth water, and therefore the warming of Antarctica (Toggweiler & Russell 2008; Toggweiler & Lea 2010). Banderas *et al.* (2012), Burke & Robinson (2012) and Kwon *et al.* (2012) support this theory by inferring increased deep-water mixing and less stratification of the water column in the Southern Ocean during the deglacial period. Anderson *et al.* (2009) also interpreted biogenic opal flux as an upwelling proxy because biogenic opal production is ultimately limited by dissolved Si supply, explaining its direct, but not necessarily linear connection. Biogenic opal mass accumulation rate rose abruptly at MD07-3133 and still also the ^{230}Th-normalized biogenic opal flux record of MD07-3134 (Fig. 5e, *g*, grey vertical bar) rose around 17 ka, thus representing probable increases in bioproductivity and upwelling. The rise is followed by a maximum around 15 ka in biogenic opal accumulation rate at MD07-3133, which was also detected at other core sites in the Southern Ocean (Atlantic, Indian, and Pacific sectors; Anderson *et al.* 2009), and coincides with Antarctic Isotopic Maximum 1.

During the Antarctic Cold Reversal (14.54–12.76 ka; Putnam *et al.* 2010), biogenic opal mass accumulation rates at MD07-3133 and

MD07-3134 (Fig. 5e) are only slightly reduced and remain high. Also EDML ice core data show only a minor reduction in $\delta^{18}O$ and rise in sea-salt Na^+ flux (Fig. 5a, b) according to regional differences. This is slightly different from the observation of Anderson *et al.* (2009) of strongly decreased biogenic opal flux (Fig. 5g), indicating reduced Southern Ocean upwelling during that time. The Antarctic Cold Reversal is followed by the Antarctic Isotopic Maximum 0, an abrupt rise in temperature and CO_2, as well as sea ice decrease; also the biogenic opal content rose at both core sites during that time.

Linear sedimentation rate and biogenic opal mass accumulation rate were equivalent for both Scotia Sea sites during the Last Glacial Maximum but increased by a factor of 1.5–2 at site MD07-3133 during MIS 3, the Antarctic Cold Reversal and MIS 1 (Fig. 4a, e). Higher amplitudes further north could be related to an approximately 5° shift in latitude of the Antarctic Circumpolar Current fronts (and associated opal belt) to the north during the Last Glacial Maximum (Gersonde *et al.* 2003). Also, Allen *et al.* (2011) observed a shift of the winter sea ice limit of at least 5° northwards during the Last Glacial Maximum, so that it remained north of the Scotia Sea. Accordingly, at that time, both core sites would have been within the winter sea ice limit, explaining the similarly reduced biogenic opal mass accumulation and linear sedimentation rates. Today, MD07-3133, which is located approximately 450 km NW of MD07-3134 (Fig. 1), lies north of the winter sea ice limit with significantly elevated biogenic opal mass accumulation and linear sedimentation rates, while MD07-3134 is within the winter sea ice limit and exhibits reduced biogenic opal mass accumulation and linear sedimentation rates. Therefore, we suggest that the distribution of sea ice has a strong influence on bioproductivity and could be the reason for pronounced regional differences in the Southern Ocean.

The last glacial period was characterized by abrupt millennial-scale climate fluctuations (e.g. Blunier & Brook 2001; Ahn & Brook 2008), which have been detected worldwide, for example in stalagmites in SE China (Cosford *et al.* 2008), in Antarctic ice cores (e.g. EDML; EPICA Community Members 2006; Fig. 5a, b) and in Greenland ice cores (nGRIP; NGRIP Members 2004; Fig. 5h). Also, in marine sediments (ODP site 1089; Cortese & Abelmann 2002; Fig. 5d) in the Atlantic Sector, the summer sea surface temperature record shows large millennial-scale temperature changes during the last glacial and correlates relatively well with our biogenic opal percentages, and to a lesser extent also with the biogenic opal mass accumulation rate records. During periods with high summer sea surface temperature, maxima in biogenic opal percentages can also be recognized. Around 65 ka in MIS 4 the MD07-3134 data show an absolute maximum in biogenic opal percentages, which is also observed in the ^{230}Th-normalized biogenic opal flux (Fig. 5g). At this time, summer sea surface temperature at ODP site 1089 (Cortese & Abelmann 2002; Fig. 5d), in the Atlantic Sector, also rose about 4 °C.

The precise and detailed chronology of sites MD07-3133 and MD07-3134 in combination with the decadal-scale resolution of biogenic opal determinations provides the opportunity to study regional bioproductivity changes in the Southern Ocean relative to the timing of individual Antarctic Isotopic Maxima. Strong high-frequency fluctuations are also noticeable in the biogenic opal content record (Fig. 5f) and to a lesser extent in biogenic opal mass accumulation rate (Fig. 5e). At site MD07-3134, biogenic opal peaks, representing enhanced bioproductivity, occurred during the relatively warm phases in Antarctica, that is, during Antarctic Isotopic Maxima 5, 7, 8, 10, 12, 13, 14, 16, 17 and 19, while less sea ice occurred (Fig. 5b). Extremely large spikes are documented for Antarctic Isotopic Maxima 15, 18, 20 and 22, when the biogenic opal mass accumulation rate in the central Scotia Sea increases up to more than 20 g cm^{-2} kyr^{-1}, at times when the sea ice cover was only marginally reduced and Antarctic atmospheric temperatures and CO_2 concentration elevated only slightly. These fluxes are, however, clearly biased by sediment focusing as stated by the ^{230}Th normalization results (Fig. 4c, d), but still showing the same incline. In general, biogenic opal content and mass accumulation rates show the same trend as atmospheric CO_2 concentration (Fig. 5c); biogenic opal rises correspond well to increasing CO_2 concentration, while during low CO_2, biogenic opal is also mainly at minima. In addition, Anderson *et al.* (2009) also found an increase in upwelling at each phase of rising CO_2 during MIS 3, illustrated by higher biogenic opal flux in the Southern Ocean (Fig. 5g, blue and grey curve), which corresponds quite well with the ^{230}Th normalized biogenic opal flux from MD07-3134 (Fig. 5g, black curve). Our investigations show that variations in biogenic opal flux reflect bioproductivity changes and strongly correlate to sea ice cover, summer sea surface temperature as well as atmospheric CO_2 variations.

Summary and conclusions

Silica is an important nutrient that fuels biological production in the Southern Ocean. We investigated two long deep-sea sediment cores from the central

Scotia Sea south of the present Antarctic Polar Front, that exhibit exceptionally high sedimentation rates (up to 1.8 and 1.2 m kyr^{-1} for sites MD07-3133 and MD07-3134, respectively) to gain detailed (decadal-scale) insight into past biogenic opal flux variations.

In a first step, we measured biogenic opal conventionally by leaching 253 samples from core sections providing large-amplitude variations according to the method of Müller & Schneider (1993). Then we estimated biogenic opal by testing three methods that rely on *c.* 9100 non-destructive measurements (at 1 cm increments) of sediment colour b^*, wet bulk density and Si/Ti-count ratios. Finally, we determined biogenic opal using FTIRS on 891 samples at 10 cm increments.

One interesting result is that all methods can be used to decipher general biogenic opal trends. However, FTIRS – a novel method for marine sediment – provides the most reliable estimation relative to the conventional leaching method. It is rather inexpensive and requires only a small portion (11 mg) of sample material.

Biogenic opal flux records in the Southern Ocean are only marginally affected by preservation changes and therefore provide valid information on past bioproductivity changes. We provide the first decadal-scale resolution continuous bioproductivity record for the Southern Ocean over the last 92.5 kyr. The biogenic opal mass accumulation rate records of the central Scotia Sea exhibit a relatively complicated glacial-to-interglacial pattern with large-amplitude, millennial-scale fluctuations in bioproductivity.

South of the Antarctic Polar Front, lowest bioproductivity levels deduced from biogenic opal fluxes occurred during the Last Glacial Maximum, when upwelling of mid-depth water was reduced and sea ice cover intensified. ^{230}Th normalized biogenic opal fluxes in core MD07-3134 show a similar pattern albeit at realistic values of between 1 and 1.5 g cm^{-2} kyr^{-1} during interglacials, whereas glacial MIS 2 and 3 were generally characterized by lower values near 0.5 g cm^{-2} kyr^{-1}. These numbers are comparable to other records in the Atlantic sector of the Southern Ocean. Around 17 ka, bioproductivity increased abruptly, corresponding to rising atmospheric CO_2 and decreasing seasonal sea ice coverage. Distribution of sea ice strongly influences bioproductivity and may be the reason for pronounced regional differences in the Southern Ocean. Also summer sea surface temperature changes are strongly correlated to the biogenic opal flux changes in the central Scotia Sea.

We are grateful for financial support from the Deutsche Forschungsgemeinschaft (DFG; grants RI 525/17-1, KU 683/9-1, WE2039/8-1) and the DFG-Priority Programme Antarctic Research 1158. Thanks are also due to C. Olofsson and C. Meyer-Jacob for assisting the FTIRS measurements at Climate Impacts Research Centre in Umeå, Sweden. A. Kolevica is thanked for the U-series isotope measurements on the quadrupole ICPMS at GEOMAR, Kiel. Finally, we thank the reviewers R. Anderson and X. Crosta, who greatly helped to improve the manuscript. Our study was part of the Southern Ocean Initiative of the International Marine Past Global Change Study programme and the AWI research programme 'Polar Regions and Coasts in a changing Earth System', Topic 3, 'Lessons from the Past'. Supplementary data to this paper are available at http://doi.pangaea.de/10.1594/PANGAEA.789348.

References

Ahn, J. & Brook, E. J. 2008. Atmospheric CO_2 and climate on millennial time scales during the last glacial period. *Science*, **322**, 83–85.

Allen, C. S., Pike, J. & Pudsey, C. J. 2011. Last glacial–interglacial sea-ice cover in the SW Atlantic and its potential role in global deglaciation. *Quaternary Science Reviews*, **30**, 2446–2458.

Anderson, J. B. & Andrews, J. T. 1999. Radiocarbon constraints on ice sheet advance and retreat in the Weddell Sea, Antarctica. *Geology*, **27**, 179–182.

Anderson, R. F., Ali, S., Bradtmiller, L. I., Nielsen, S. H. H., Fleisher, M. Q., Anderson, B. E. & Burckle, L. H. 2009. Wind-driven upwelling in the Southern Ocean and the deglacial rise in atmospheric CO_2. *Science*, **323**, 1443–1448.

Balascio, N. L., Zhang, Z., Bradley, R. S., Perren, B., Dahl, S. O. & Bakke, J. 2011. A multi-proxy approach to assessing isolation basin stratigraphy from the Lofoten Islands, Norway. *Quaternary Research*, **75**, 288–300.

Banderas, R., Álvarez-Solas, J. & Montoya, M. 2012. Role of CO_2 and Southern Ocean winds in glacial abrupt climate change. *Climate of the Past*, **8**, 1011–1021.

Bareille, G., Labracherie, M., Bertrand, P., Labeyrie, L., Lavaux, G. & Dignan, M. 1998. Glacial–interglacial changes in the accumulation rates of major biogenic components in Southern Indian Ocean sediments. *Journal of Marine Systems*, **17**, 527–539.

Berger, A. & Loutre, M. F. 1991. Insolation values for the climate of the last 10 million years. *Quaternary Science Reviews*, **10**, 297–317.

Blunier, T. & Brook, E. J. 2001. Timing of millennial-scale climate change in Antarctica and Greenland during the last glacial period. *Science*, **291**, 109–112.

Boyd, P. W., Watson, A. J. *et al.* 2000. A mesoscale phytoplankton bloom in the polar Southern Ocean stimulated by iron fertilization. *Nature*, **407**, 695–702.

Bradtmiller, L. I., Anderson, R. F., Fleisher, M. Q. & Burckle, L. H. 2007. Opal burial in the equatorial Atlantic Ocean over the last 30 ka: implications for glacial–interglacial changes in the ocean silicon cycle. *Paleoceanography*, **22**, PA4216, doi: 10.1029/2007PA001443.

Bradtmiller, L. I., Anderson, R. F., Fleisher, M. Q. & Burckle, L. H. 2009. Comparing glacial and

Holocene opal fluxes in the Pacific sector of the Southern Ocean. *Palaeoceanography*, **24**, PA2214, doi: 10.1029/2008PA001693.

Burke, A. & Robinson, L. F. 2012. The Southern Ocean's role in carbon exchange during the last deglaciation. *Science*, **335**, 557–561.

Cassar, N., Bender, M. L., Barnett, B. A., Fan, S., Moxim, W. J., Levy Ii, H. & Tilbrook, B. 2007. The Southern Ocean biological response to aeolian iron deposition. *Science*, **317**, 1067–1070.

Charles, C. D., Froelich, P. N., Zibello, M. A., Mortlock, R. A. & Morley, J. J. 1991. Biogenic opal in southern ocean sediments over the last 450 000 years: implications for surface water chemistry and circulation. *Paleoceanography*, **6**, 697–728, doi: 10.1029/91PA02477.

Chase, Z., Anderson, R. F., Fleisher, M. Q. & Kubik, P. W. 2003. Accumulation of biogenic and lithogenic material in the Pacific sector of the Southern Ocean during the past 40 000 years. *Deep Sea Research II*, **50**, 799–832.

Cortese, G. & Abelmann, A. 2002. Radiolarian-based paleotemperatures during the last 160 kyr at ODP Site 1089 (Southern Ocean, Atlantic Sector). *Palaeogeography, Palaeoclimatology, Palaeoecology*, **182**, 259–286.

Cosford, J., Qing, H., Yuan, D., Zhang, M., Holmden, C., Patterson, W. & Hai, C. 2008. Millennial-scale variability in the Asian monsoon: evidence from oxygen isotope records from stalagmites in south-eastern China. *Palaeogeography, Palaeoclimatology, Palaeoecology*, **266**, 3–12.

de Baar, H. J. W., Boyd, P. W. *et al.* 2005. Synthesis of iron fertilization experiments: from the iron age in the age of enlightenment. *Journal of Geophysical Research: Oceans*, **110**, C9, C09S16, doi: 10.1029/2004jc002601

Delmonte, B., Petit, J. R., Andersen, K. K., Basile-Doelsch, I., Maggi, V. & Ya Lipenkov, V. 2004. Dust size evidence for opposite regional atmospheric circulation changes over east Antarctica during the last climatic transition. *Climate Dynamics*, **23**, 427–438.

Denton, G. H., Anderson, R. F., Toggweiler, J. R., Edwards, R. L., Schaefer, J. M. & Putnam, A. E. 2010. The last glacial termination. *Science*, **328**, 1652–1656.

Dezileau, L., Reyss, J. L. & Lemoine, F. 2003. Late Quaternary changes in biogenic opal fluxes in the Southern Indian Ocean. *Marine Geology*, **202**, 143–158.

Diekmann, B. 2007. Sedimentary patterns in the late Quaternary Southern Ocean. *Deep Sea Research II*, **54**, 2350–2366.

Diekmann, B., Kuhn, G. *et al.* 2000. Terrigenous sediment supply in the Scotia Sea (Southern Ocean): response to Late Quaternary ice dynamics in Patagonia and on the Antarctic Peninsula. *Palaeogeography, Palaeoclimatology, Palaeoecology*, **162**, 357–387.

EPICA COMMUNITY MEMBERS 2004. Eight glacial cycles from an Antarctic ice core. *Nature*, **429**, 623–628.

EPICA COMMUNITY MEMBERS 2006. One-to-one coupling of glacial climate variability in Greenland and Antarctica. *Nature*, **444**, 195–198.

Erickson, D. J., Hernandez, J. L., Ginoux, P., Gregg, W. W., McClain, C. & Christian, J. 2003. Atmospheric iron delivery and surface ocean biological activity in the Southern Ocean and Patagonian region. *Geophysical Research Letters*, **30**, 12, 1609, doi: 10.1029/2003GL017241.

Fischer, H., Fundel, F. *et al.* 2007*a*. EPICA EDML chemical concentrations and fluxes. doi: 10.1594/PANGAEA.683642

Fischer, H., Fundel, F. *et al.* 2007*b*. Reconstruction of millennial changes in dust emission, transport and regional sea ice coverage using the deep EPICA ice cores from the Atlantic and Indian Ocean sector of Antarctica. *Earth and Planetary Science Letters*, **260**, 340–354.

Francois, R., Frank, M., Rutgers van der Loeff, M. M. & Bacon, M. P. 2004. ^{230}Th normalization: an essential tool for interpreting sedimentary fluxes during the late Quaternary. *Paleoceanography*, **19**, PA1018, doi: 10.1029/2003PA000939.

Francus, P., Lamb, H., Nakagawa, T., Marshall, M., Brown, E. & Members, S. P. 2009. The potential of high-resolution X-ray fluorescence core scanning: applications in paleolimnology. *PAGES news*, **17**, 93–95.

Frank, M., Gersonde, R., Rutgers van der Loeff, M. M., Kuhn, G. & Mangini, A. 1996. Late Quaternary sediment dating and quantification of lateral sediment redistribution applying ^{230}Th$_{ex}$: a study from the eastern Atlantic sector of the Southern Ocean. *Geologische Rundschau*, **85**, 554–566.

Frank, M., Gersonde, R. & Mangini, A. 1999. Sediment redistribution, ^{230}Th$_{ex}$-normalization and implications for the reconstruction of particle flux and export paleoproductivity. *In*: Fischer, G. & Wefer, G. (eds) *Use of Proxies in Paleoceanography: Examples from the South Atlantic*. Springer, New York, 409–426.

Frank, M., Gersonde, R. *et al.* 2000. Similar glacial and interglacial export bioproductivity in the Atlantic sector of the Southern Ocean: multiproxy evidence and implications for glacial atmospheric CO_2. *Paleoceanography*, **15**, 642–658, doi: 10.1029/2000PA000497.

Geibert, W., van der Loeff, M. M. R., Usbeck, R., Gersonde, R., Kuhn, G. & Seeberg-Elverfeldt, J. 2005. Quantifying the opal belt in the Atlantic and southeast Pacific sector of the Southern Ocean by means of ^{230}Th normalization. *Global Biogeochemical Cycles*, **19**, GB4001, doi: 10.1029/2005GB002465.

Geladi, P., MacDougall, D. & Martens, H. 1985. Linearization and scatter-correction for near-infrared reflectance spectra of meat. *Applied Spectroscopy*, **39**, 491–500.

Gersonde, R., Abelmann, A. *et al.* 2003. Last glacial sea surface temperatures and sea-ice extent in the Southern Ocean (Atlantic–Indian sector): a multiproxy approach. *Paleoceanography*, **18**(3), 1061, doi: 10.1029/2002PA000809.

Gersonde, R., Crosta, X., Abelmann, A. & Armand, L. 2005. Sea-surface temperature and sea ice distribution of the Southern Ocean at the EPILOG Last Glacial Maximum – a circum-Antarctic view based on siliceous microfossil records. *Quaternary Science Reviews*, **24**, 869–896.

EDQ1

Griffiths, P. R. & De Haseth, J. A. 1986. *Fourier Transform Infrared Spectrometry*. Wiley, New York.

Guillou, H., Singer, B. S., Laj, C., Kissel, C., Scaillet, S. & Jicha, B. R. 2004. On the age of the Laschamp geomagnetic excursion. *Earth and Planetary Science Letters*, **227**, 331–343.

Hendry, K. R., Rickaby, R. E. M. & Allen, C. S. 2011. Changes in micronutrient supply to the surface Southern Ocean (Atlantic sector) across the glacial termination. *Geochemistry Geophysics Geosystems*, **12**, Q09007, doi: 10.1029/2011gc003691.

Horn, M. G., Beucher, C. P., Robinson, R. S. & Brzezinski, M. A. 2011. Southern ocean nitrogen and silicon dynamics during the last deglaciation. *Earth and Planetary Science Letters*, **310**, 334–339.

Jansen, J. H. F., Van der Gaast, S. J., Koster, B. & Vaars, A. J. 1998. CORTEX, a shipboard XRF-scanner for element analyses in split sediment cores. *Marine Geology*, **151**, 143–153.

Johnson, C. M., Brown, E. T. & Shi, J. 2011. Biogenic silica deposition in Lake Malawi, East Africa over the past 150 000 years. *Palaeogeography, Palaeoclimatology, Palaeoecology*, **303**, 103–109.

Kanfoush, S. l., Hodell, D. A., Charles, C. D., Guilderson, T. P., Mortyn, P. G. & Ninnemann, U. S. 2000. Millennial-scale instability of the Antarctic ice sheet during the last glaciation. *Science*, **288**, 1815–1818.

Kaufmann, P., Fundel, F. *et al.* 2010. Ammonium and non-sea salt sulfate in the EPICA ice cores as indicator of biological activity in the Southern Ocean. *Quaternary Science Reviews*, **29**, 313–323.

Kretschmer, S., Geibert, W., Rutgers van der Loeff, M. M., Schnabel, C., Xu, S. & Mollenhauer, G. 2011. Fractionation of ^{230}Th, ^{231}Pa, and ^{10}Be induced by particle size and composition within an opal-rich sediment of the Atlantic Southern Ocean. *Geochimica et Cosmochimica Acta*, **75**, 6971–6987.

Kumar, N., Anderson, R. F., Mortlock, R. A., Froelich, P. N., Kubik, P., Dittrich-Hannen, B. & Suter, M. 1995. Increased biological productivity and export production in the glacial Southern Ocean. *Nature*, **378**, 675–680.

Kwon, E. Y., Hain, M. P., Sigman, D. M., Galbraith, E. D., Sarmiento, J. L. & Toggweiler, J. R. 2012. North Atlantic ventilation of 'southern-sourced' deep water in the glacial ocean. *Paleoceanography*, **27**, PA2208, doi: 10.1029/2011pa002211

Lefèvre, N. & Watson, A. J. 1999. Modeling the geochemical cycle of iron in the oceans and its impact on atmospheric CO_2 concentrations. *Global Biogeochemical Cycles*, **13**, 727–736, doi: 10.1029/1999GB900034.

Li, F., Ginoux, P. & Ramaswamy, V. 2010. Transport of Patagonian dust to Antarctica. *Journal of Geophysical Research*, **115**, D18217, doi: 10.1029/2009jd012356

Lin, H., Rauschenberg, S., Hexel, C. R., Shaw, T. J. & Twining, B. S. 2011. Free-drifting icebergs as sources of iron to the Weddell Sea. *Deep-Sea Research Part II*, **58**, 1392–1406.

Lisiecki, L. E. & Raymo, M. E. 2005. A Pliocene-Pleistocene stack of 57 globally distributed benthic d^{18}O records. *Paleoceanography*, **20**, PA1003, doi: 10.1029/2004pa001071.

Maldonado, A., Barnolas, A. *et al.* 2003. Contourite deposits in the central Scotia Sea: the importance of the Antarctic Circumpolar Current and the Weddell Gyre flows. *Palaeogeography, Palaeoclimatology, Palaeoecology*, **198**, 187–221.

Martens, H. & Naes, T. 1989. *Multivariate Calibration*. John Wiley, New York.

Martin, J. H., Gordon, R. M. & Fitzwater, S. E. 1990. Iron in Antarctic waters. *Nature*, **345**, 156–158.

Martínez-Garcia, A., Rosell-Mele, A., Jaccard, S. L., Geibert, W., Sigman, D. M. & Haug, G. H. 2011. Southern Ocean dust-climate coupling over the past four million years. *Nature*, **476**, 312–315.

Meskhidze, N., Nenes, A., Chameides, W. L., Luo, C. & Mahowald, N. 2007. Atlantic Southern Ocean productivity: fertilization from above or below? *Global Biogeochemical Cycles*, **21**, GB2006, doi: 10.1029/2006GB002711.

Monnin, E. 2006. EPICA Dome C high resolution carbon dioxide concentrations, doi: 10.1594/PANGAEA. 472488.

Moreno, P. I., Lowell, T. V., Jacobson, G. L., Jr & Denton, G. H. 1999. Abrupt vegetation and climate changes during the Last glacial Maximum and Last Termination in the Chilean Lake District: a case study from Canal De La Puntilla (41°S). *Geografiska Annaler: Series A, Physical Geography*, **81**, 285–311.

Mortlock, R. A., Charles, C. D., Froelich, P. N., Zibello, M. A., Saltzman, J., Hays, J. D. & Burckle, L. H. 1991. Evidence for lower productivity in the Antarctic Ocean during the last glaciation. *Nature*, **351**, 220–223.

Müller, P. J. & Schneider, R. 1993. An automated leaching method for the determination of opal in sediments and particulate matter. *Deep Sea Research I*, **40**, 425–444.

Murray, R. W., Leinen, M. & Isern, A. R. 1993. Biogenic flux of Al to sediment in the central equatorial Pacific Ocean: evidence for increased productivity during glacial periods. *Paleoceanography*, **8**, 651–670, doi: 10.1029/93PA02195

NGRIP MEMBERS. 2004. High-resolution record of Northern Hemisphere climate extending into the last interglacial period. *Nature*, **431**, 147–151.

Nielsen, S. H. H., Hodell, D. A., Kamenov, G., Guilderson, T. & Perfit, M. R. 2007. Origin and significance of ice-rafted detritus in the Atlantic sector of the Southern Ocean. *Geochemistry, Geophysics, Geosystems*, **8**, Q12005, doi: 10.1029/2007GC001618

Orsi, A. H., Whitworth, T. III & Nowlin, W. D. Jr. 1995. On the meridional extent and fronts of the Antarctic Circumpolar Current. *Deep Sea Research I*, **42**, 641–673.

Paillard, D., Labeyrie, L. & Yiou, P. 1996. Macintosh Program performs time-series analysis. *EOS Transactions*, **77**, 379–379, doi: 10.1029/96eo00259

Pondaven, P., Ragueneau, O., Treguer, P., Hauvespre, A., Dezileau, L. & Reyss, J. L. 2000. Resolving the 'opal paradox' in the Southern Ocean. *Nature*, **405**, 168–172.

Pudsey, C. J. & Howe, J. A. 1998. Quaternary history of the Antarctic Circumpolar Current: evidence from the Scotia Sea. *Marine Geology*, **148**, 83–112.

Pugh, R. S., McCave, I. N., Hillenbrand, C. D. & Kuhn, G. 2009. Circum-Antarctic age modelling of Quaternary marine cores under the Antarctic Circumpolar Current: ice-core dust–magnetic correlation. *Earth and Planetary Science Letters*, **284**, 113–123.

Putnam, A. E., Denton, G. H. *et al.* 2010. Glacier advance in southern middle-latitudes during the Antarctic Cold Reversal. *Nature Geoscience*, **3**, 700–704.

Ragueneau, O., Treguer, P. *et al.* 2000. A review of the Si cycle in the modern ocean: recent progress and missing gaps in the application of biogenic opal as a paleoproductivity proxy. *Global and Planetary Change*, 317–365.

Rahmstorf, S. 2002. Ocean circulation and climate during the past 120 000 years. *Nature*, **419**, 207–214.

Raiswell, R. 2011. Iceberg-hosted nanoparticulate Fe in the Southern Ocean: mineralogy, origin, dissolution kinetics and source of bioavailable Fe. *Deep Sea Research Part II*, **58**, 1364–1375.

Richter, T. O., van der Gaast, S. *et al.* 2006. The Avaatech XRF Core Scanner: technical description and applications to NE Atlantic sediments. *Geological Society, London, Special Publications*, **267**, 39–50.

Rosén, P., Vogel, H., Cunningham, L., Reuss, N., Conley, D. J. & Persson, P. 2010. Fourier transform infrared spectroscopy, a new method for rapid determination of total organic and inorganic carbon and biogenic silica concentration in lake sediments. *Journal of Paleolimnology*, **43**, 247–259.

Rosén, P., Vogel, H. *et al.* 2011. Universally applicable model for the quantitative determination of lake sediment composition using Fourier transform infrared spectroscopy. *Environmental Science & Technology*, **45**, 8858–8865.

Schlüter, M. & Rickert, D. 1998. Effect of pH on the measurement of biogenic silica. *Marine Chemistry*, **63**, 81–93.

Stenni, B., Masson-Delmotte, V. *et al.* 2010. The deuterium excess records of EPICA Dome C and Dronning Maud Land ice cores (East Antarctica). *Quaternary Science Reviews*, **29**, 146–159.

Stuart, K. M. & Long, D. G. 2011. Tracking large tabular icebergs using the SeaWinds Ku-band microwave scatterometer. *Deep Sea Research Part II*, **58**, 1285–1300.

Swann, G. 2010. A comparison of the Si/Al and Si/time wet-alkaline digestion methods for measurement of biogenic silica in lake sediments. *Journal of Paleolimnology*, **44**, 375–385.

Tjallingii, R., Röhl, U., Kölling, M. & Bickert, T. 2007. Influence of the water content on X-ray fluorescence core- scanning measurements in soft marine sediments. *Geochemistry, Geophysics, Geosystems*, **8**, Q02004, doi: 10.1029/2006GC001393

Toggweiler, J. R. 2009. Shifting westerlies. *Science*, **323**, 1434–1435.

Toggweiler, J. R. & Lea, D. W. 2010. Temperature differences between the hemispheres and ice age climate variability. *Paleoceanography*, **25**, PA2212, doi: 10.1029/2009pa001758

Toggweiler, J. R. & Russell, J. 2008. Ocean circulation in a warming climate. *Nature*, **451**, 286–288.

Toggweiler, J. R., Russell, J. L. & Carson, S. R. 2006. Midlatitude westerlies, atmospheric CO_2, and climate change during the ice ages. *Paleoceanography*, **21**, 15, doi: 10.1029/2005pa001154

Vogel, H., Rosén, P., Wagner, B., Melles, M. & Persson, P. 2008. Fourier transform infrared spectroscopy, a new cost-effective tool for quantitative analysis of biogeochemical properties in long sediment records. *Journal of Paleolimnology*, **40**, 689–702.

Weber, M. E. 1998. Estimation of biogenic carbonate and opal by continuous non-destructive measurements in deep-sea sediments: application to the eastern Equatorial Pacific. *Deep Sea Research I*, **45**, 1955–1975.

Weber, M. E., Niessen, F., Kuhn, G. & Wiedicke, M. 1997. Calibration and application of marine sedimentary physical properties using a multi-sensor core logger. *Marine Geology*, **136**, 151–172.

Weber, M. E., Kuhn, G., Sprenk, D., Rolf, C., Ohlwein, C. & Ricken, W. 2012. Dust transport from Patagonia to Antarctica – a new stratigraphic approach from the Scotia Sea and its implications for the last glacial cycle. *Quaternary Science Reviews*, **36**, 177–188.

Whitworth, T. & Peterson, R. G. 1985. Volume transport of the Antarctic Circumpolar Current from bottom pressure measurements. *Journal of Physical Oceanography*, **15**, 810–816.